Chemistry Europe
European Chemical Societies Publishing

Elucidating the Dual Mode of Action of Dipeptidyl Enoates in the Inhibition of Rhodesain Cysteine Proteases

Kemel Arafet,[a] Florenci V. González,[b] and Vicent Moliner*[a]

Abstract: A computational study of the two possible inhibition mechanisms of rhodesain cysteine protease by the dipeptidyl enoate Cbz-Phe-Leu-CH=CH–$CO_2C_2H_5$ has been carried out by means of molecular dynamics simulations with hybrid QM/MM potentials. The low free energy barriers confirm that the Cys25 residue can attack both C_β and C1 atoms of the inhibitor, confirming a dual mode of action in the inhibition of the rhodesain by enoates. According to the results, the inhibition process through the Cys25 attack on the C_β atom of the inhibitor is an exergonic and irreversible process, while the inhibition process when Cys25 attacks on the C1 atom of the inhibitor is and exergonic but reversible process. The interactions between the inhibitor and rhodesain suggest that P2 is the most important fragment to consider in the design of new efficient inhibitors of rhodesain. These results may be useful for the design of new inhibitors of rhodesain and other related cysteine proteases based on dipeptidyl enoates scaffolds.

Introduction

Cysteine proteases (CPs) of parasites have been shown to be involved in functions such as hemoglobin degradation, parasite egress, or processing surface proteins, thus being responsible of several human diseases.[1–3] The parasitic rhodesain CP is expressed by the protozoa *Trypanosoma brucei rhodesiense*, which is responsible for the African sleeping sickness. The disease is endemic in 36 sub-Saharan African countries and it is fatal when untreated, current treatments have several side effects.[4] Thus, rhodesain has become an attractive target for the development of new inhibitors for their medicinal interest.

In the last years, several classes of inhibitors have shown good inhibition activity against rhodesain,[5–12] including the Michael acceptors, the most studied group of inhibitors of this family of enzymes which have demonstrated efficacy in preclinical trials.[13] Based on the features of irreversible dipeptidyl vinylsulfones inhibitors,[14] González and co-workers proposed dipeptidyl enoates as alternative inhibitors of CPs.[5,10] One of these inhibitors, the dipeptidyl enoate Cbz-Phe-Leu-CH=CH–$CO_2C_2H_5$, showed a potent inhibitory activity against rhodesain with a second-order rate constant of seven orders of magnitude, 1.61×10^6 $M^{-1}\cdot s^{-1}$.[10]

In the case of dipeptidyl enoates, González and co-workers suggested a dual mode of action in the inhibition of rhodesain.[5] An irreversible inhibition mechanism through a Michael addition consisting on an attack on the β-carbon by the thiolate of the active site Cys residue followed by protonation of the α-carbon to form the thioether derivative (see mechanism I in Scheme I).[15,16] The inhibition mechanisms of different CPs by Michael acceptor inhibitors have been studied in our laboratory through quantum mechanics/molecular mechanics (QM/MM) simulations.[17,18] According to our results, the inhibition of these CPs through the Michael addition takes place in two steps, the anionic $CysS^-$ residue first attack the β-carbon of the inhibitor, leading to a stable intermediate; and then the proton from the active-site $HisH^+$ residue is transferred α-carbon of the inhibitor to form the thioether derivative. A reversible mode of action takes place through the attack of the Cys25 residue to the carbonyl carbon to give a thiohemiketal intermediate (THA) as a reversible enzyme·inhibitor complex (see mechanism II in Scheme 1). The stability of the THA intermediate has been questioned by several authors,[19–22] including ourselves according to QM/MM studies of the mechanisms of catalysis and inhibition of cruzain,[23–25] a cysteine protease that shares 70% sequence identity with rhodesain. Any attempt to explore both the inhibition of cruzain by peptidyl halomethyl ketones[23] or the acylation step in the catalytic mechanism[24,25] through the formation of the THA intermediate has been unsuccessful. However, recently the presence of the THA has been detected in the active site of the SARS-CoV-2 M^{pro} CP in both inhibition mechanism by α-ketoamide[26] and in the mechanism of proteolysis.[27]

Several authors have demonstrated that the inhibition of rhodesain is dependent on the peptidic framework of the inhibitor.[5,6,10,28–35] Diederich and co-workers,[28] in a structure-based study of nitrile-derived rhodesain inhibitors, showed that

[a] Dr. K. Arafet, Prof. V. Moliner
Institute of Advanced Materials (INAM)
Universitat Jaume I, 12071 Castelló (Spain)
E-mail: moliner@uji.es

[b] Prof. F. V. González
Departament de Química Inorgànica i Orgànica
Universitat Jaume I, 12071 Castelló (Spain)

Supporting information for this article is available on the WWW under https://doi.org/10.1002/chem.202100892

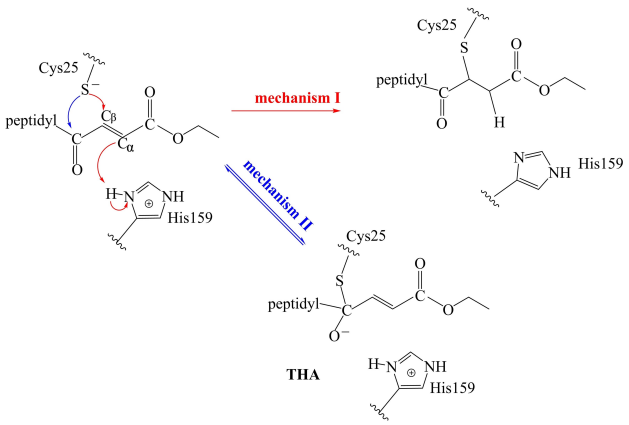

Scheme 1. Dual mode of action of dipeptidyl enoates.

variations in the S1 pocket had weak effects on selectivity of this enzyme; moreover, rhodesain preferred extended hydrophobic for its S2 pocket, while the S3 pocket shows clear preference for aromatic substituents. Later, Schirmeister and co-workers confirm these results,[31] and concluded that the interaction between the S2 pocket of rhodesain and the P2 residue of the inhibitor is an important specificity determinant. In addition, they showed that the absence of hydrogen bond interactions with the residues Gly66 and Asp158 is related with a lower affinity of the inhibitor. Recently, Ettari and co-workers in a structural study with novel peptide-based Michael acceptor inhibitors arrived to some conclusions based on structural variations on the P3, P2, and P1′ sites in the inhibitor.[33] The substitution pattern on the phenyl at the P3 position has a remarkable impact on the inhibition of the target protease, being the optimal substitution pattern the presence of electron withdrawing fluorine atom or CF_3 group located at 2 or 4 positions. With respect to the P2 site, the substitution of the Phe residue with a homophenylalanine decreased the inhibitory properties. They observed the same behaviour when the methyl group of the vinyl ketone warhead at the P1′ site of the inhibitor was replaced with an ethyl group. In the case of dipeptidyl enoate inhibitors, rhodesain exhibits a preference for the Phe residue at the P2 site[5] and for the Leu residue in the P1 site[10] of the inhibitor. More recently, Neuweiler and co-workers found in the irreversible vinylsulfones inhibitors, a highly reactive warhead increases the efficiency of the rhodesain inhibition.[36]

Herein, we reported a detailed QM/MM study of the inhibition mechanisms of rhodesain cysteine protease by the dipeptidyl enoate Cbz-Phe-Leu-CH=CH–$CO_2C_2H_5$. The analysis of the free energy surface (FES) of every single chemical step, computed in terms of the potential of mean force (PMF), and the interactions between the inhibitor and the protein afford describing how dipeptidyl enoate inhibits this CP at atomistic level, and proposing suggestions for the design of new inhibitors of cysteine proteases with increasing affinity and selectivity.

Results and Discussion

As mentioned in the previous section, the inhibition mechanism of the rhodesain CP by the dipeptidyl enoate Cbz-Phe-Leu-CH=CH–$CO_2C_2H_5$ has been studied by the generation of the FESs corresponding to two possible mechanisms (see Scheme 1): the nucleophilic attack of Cys25 on the C_β of the inhibitor (Mechanism I) or on the carbonyl carbon C1 of the inhibitor (Mechanism II).

Inhibition mechanism I

The M06-2X:AM1d/MM FESs corresponding to the full inhibition mechanism I is shown in Figure 1.

The corresponding PMFs at the AM1d/MM level is deposited in the Supporting Information (see Figure S3). As observed, the FESs confirms the step-wise character of the mechanism: first the Cys25 of the protein attacks on the C_β atom of the inhibitor, leading to a stable intermediate Int-C_β (see Scheme 2) and then the proton from His159 is transferred to the C_α atom of the inhibitor forming the PS-C_β. According to the results, the attack

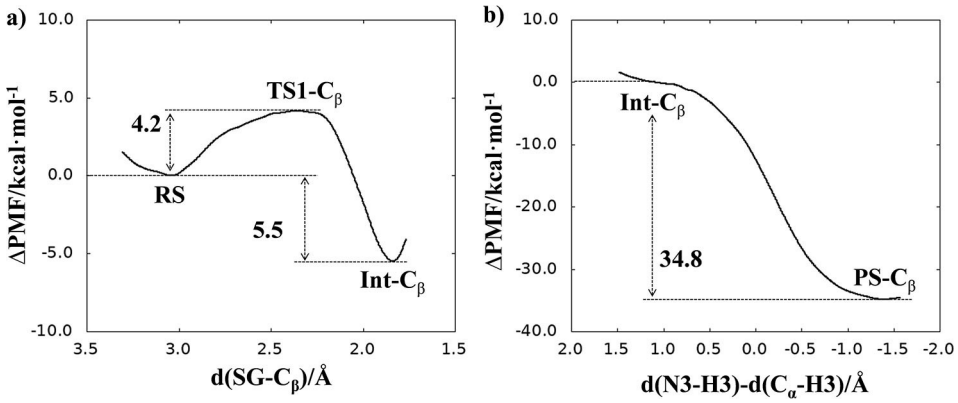

Figure 1. M06-2X/6-31 + G(d,p):AM1d/MM FES for the inhibition mechanism I. a) Attack of sulfur on C_β. b) Protonation of the Int-C_β intermediate.

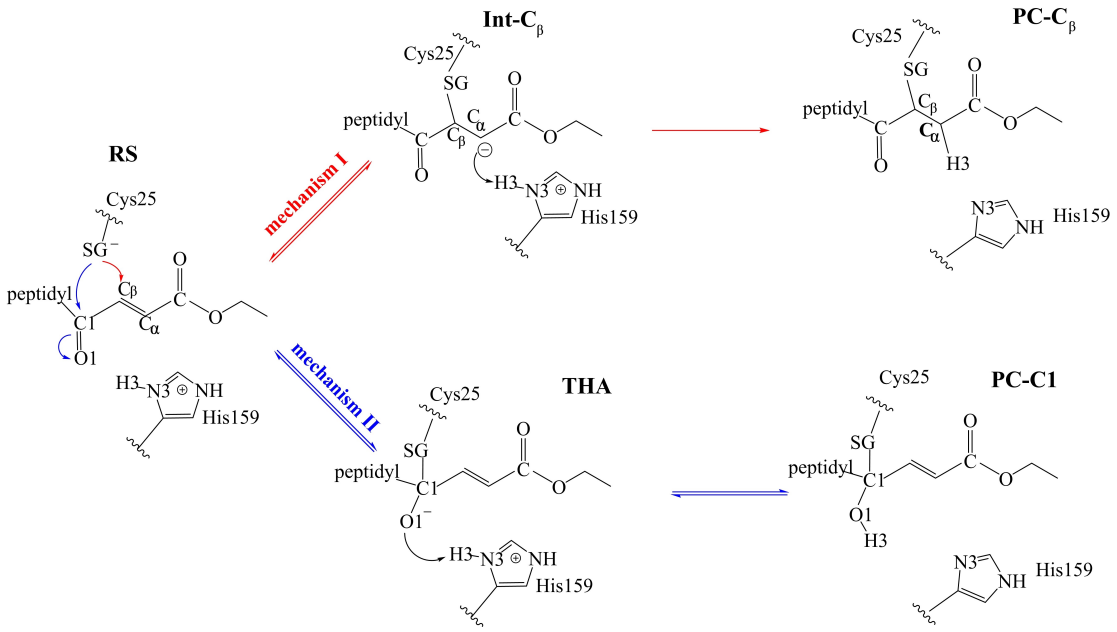

Scheme 2. Proposed inhibition mechanisms of rhodesain by dipeptidyl enoates as deduced from M06-2X/6-31 + G(d,p):AM1d/MM calculations.

of Cys25 on the C_β, through TS1-C_β, proceeds with a free energy barrier of 4.2 kcal·mol^{-1} (see Figure 1a). Then, the proton transfer from His159 to the C_α atom of the inhibitor takes place in a barrierless fashion leading to a stable PS-C_β. The formation of the intermediate Int-C_β is the rate-limiting step of the inhibition process. The structure of the TS1-C_β was optimized at M06-2X/6-31 + G(d,p)/MM level and the minimum energy path, computed as the intrinsic reaction coordinate (IRC) path, confirms the predictions derived from the M06-2X:AM1d/MM FES (see Table S1).

From a thermodynamic point of view, an important difference is observed between the two steps of the inhibition process (see Figure 1), while the formation of the intermediate Int-C_β is a reversible process the second step has a clear irreversible character, being the full inhibition process exergonic with a value of the reaction free energy of −40.3 kcal·mol^{-1}.

Representative snapshots of the key states involved in the inhibition mechanism I are presented in Figure 2, while the average values of the key interatomic distances are listed in Table S2 (see Supporting Information). The geometrical analysis indicates that while the SG–C_β bond is forming (2.39 ± 0.03 Å)

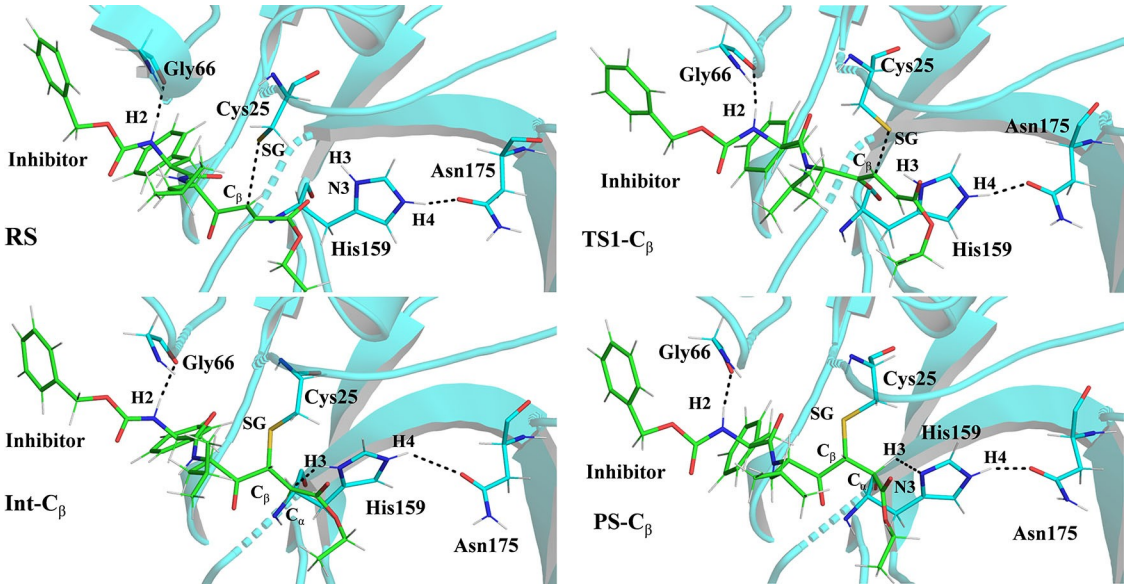

Figure 2. Representative snapshots of the key states of the inhibition mechanism I.

in TS1, the double bond between C_β and C_α remains almost unaltered (1.34 ± 0.02 Å and 1.36 ± 0.02 Å in RS and TS1-C_β, respectively). The value of the C_β–C_α distance in the PS is typical of a single C–C bond (1.53 ± 0.03 Å). It is important to note how in the RS complex, the transferring hydrogen atom of His159 is far from the C_α of the inhibitor, d(C_α-H3) = 5.59 ± 0.34 Å. Nevertheless, as the double C_β–C_α bond is elongating, the His159 is approaching to a more reactive position being the distance C_α–H3 equal to 2.09 ± 0.22 Å in the intermediate Int-C_β.

As mentioned before, a QM/MM study of the inhibition mechanism of cysteine protease rhodesain by a dipeptidyl nitroalkene, Cbz-Phe-Ala-CH=CH–NO_2, was recently carried out in our laboratory.[17] Thus, a comparative analysis between the reactivity of the two families of inhibitors (dipeptidyl nitroalkenes vs dipeptidyl enoates) toward rhodesain can be based on the obtained free energy profiles. In this sense, the reactivity of the dipeptidyl enoate Cbz-Phe-Leu-CH=CH–$CO_2C_2H_5$ is greater than that of the dipeptidyl nitroalkene Cbz-Phe-Ala-CH=CH-NO_2 because the free energy barrier of the inhibition with the enoate is significantly lower than the one required to form the covalent linkage between the protein and the nitroalkene (4.2 kcal·mol^{-1} vs 20.4 kcal·mol^{-1}).

Inhibition mechanism II

The second proposed inhibition mechanism consists of the sulfur attack on the carbonyl carbon C1 (see Scheme 2). The M06-2X:AM1d/MM 2D-FES corresponding to the full inhibition process is shown in Figure 3.

The corresponding PMF at the AM1d/MM level, and the average values of key interatomic distances are deposited in the Supporting Information (see Figure S6b and Table S3, respectively). Representative snapshots of some key states involved in the inhibition process are presented in Figure 4. The first conclusion derived from the FES shown in Figure 3 is that the inhibition mechanism takes place in two steps, first the Cys25 of the protein attacks on the C1 atom of the inhibitor through TS1-C1, with a free energy barrier of 2.0 kcal·mol^{-1},

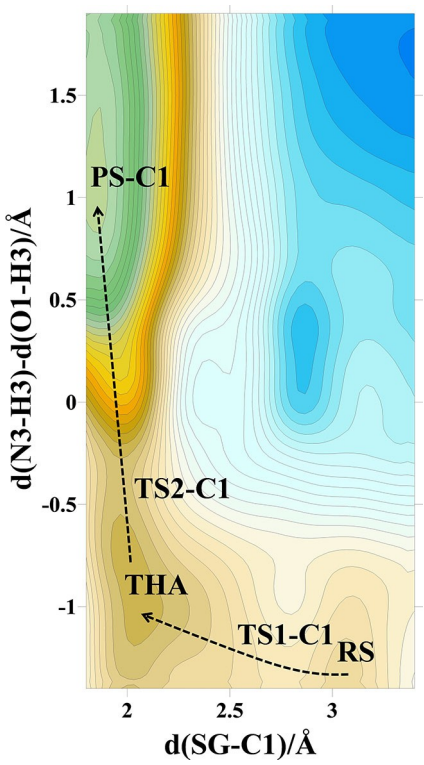

Figure 3. M06-2X/6-31 + G(d,p):AM1d/MM FES of the inhibition mechanism II. Iso-energetic lines are displayed every 1.0 kcal·mol^{-1}.

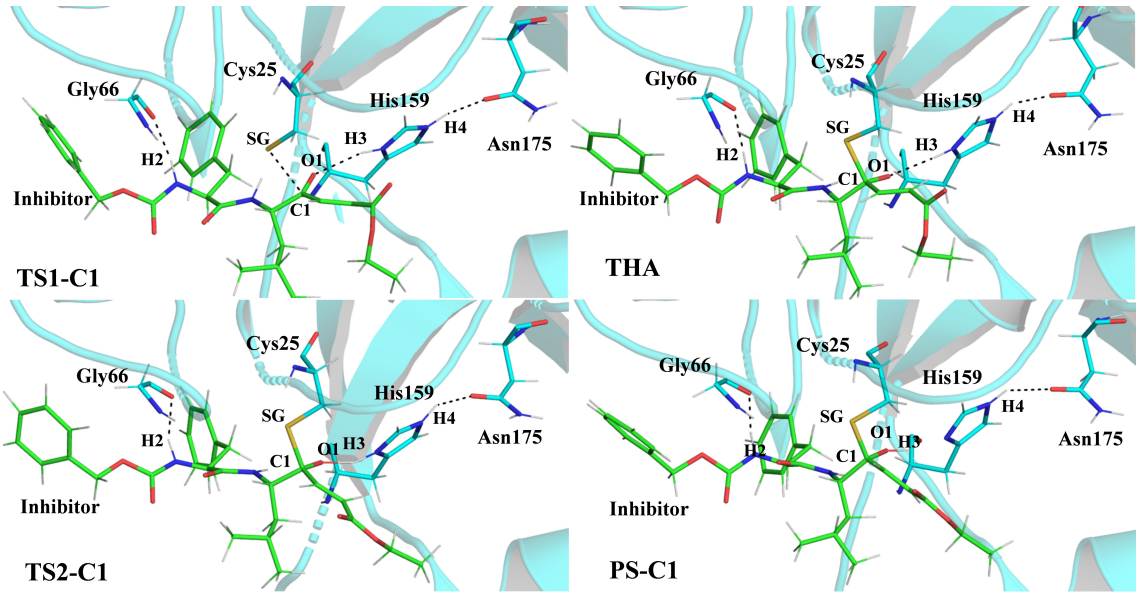

Figure 4. Representative snapshots of the key states of the inhibition mechanism II.

leading to the stable intermediate THA. Later, the proton from His159 is transferred to the O1 atom of the inhibitor forming the PS–C1. This second step takes place through TS2-C1, with a low free energy barrier of 0.9 kcal·mol^{-1}. The whole inhibition process is exergonic with a value of the reaction free energy of −21.8 kcal·mol^{-1}. An interesting point in this second mode of action of the enoate inhibitors is the presence of the metastable THA intermediate, 2.9 kcal·mol^{-1} more stable than the RS complex. As commented in the Introduction section, any previous attempt to explore the inhibition[23] or the acylation step in the catalytic mechanism[24,25] of the cruzain cysteine protease through the formation of the THA intermediate was unsuccessful. The structure of both TS1-C1 and TS2-C1 were optimized at M06-2X/6-31+G(d,p)/MM level and the minimum energy path, computed as the IRC path, confirms the predictions derived from the M06-2X:AM1d/MM FES (see Table S4).

Comparison between mechanism I and mechanism II

Figure 5 displays the free energy profiles of the two inhibition mechanisms of rhodesain by the dipeptidyl enoate Cbz-Phe-Leu-CH=CH–$CO_2C_2H_5$. The free energy profiles clearly indicate that the Cys25 can attack both C_β and C1 atoms, confirming a dual mode of action in the inhibition of rhodesain by the enoates, as previously suggested by González and co-workers.[5]

The first step in both cases is reversible and is related to the formation of the SG–C bond, forming two stable intermediates Int-C_β and THA, being the Int-C_β intermediate slightly more stable than the THA. From a kinetic point of view, the low free energy barrier indicates that the formation of both intermediates Int-C_β and THA is a favourable process. The low activation free energies obtained in both inhibition mechanisms are in total agreement with the second-order rate constant of seven orders of magnitude determined by González and co-workers.[10] Regarding the second step of the inhibition process, the more important difference is related to its reversibility; while the formation of the PS–C1 complex is a reversible process with a reaction free energy of −18.9 kcal·mol^{-1}, the formation of the PS-C_β complex is clearly irreversible with a reaction free energy of −34.8 kcal·mol^{-1}. The confirmation of the dual mode of action of this family of inhibitors is an important issue that can be used to design improved inhibitors. Thus, according to our results, the reversible or irreversible character of the inhibitor could be modulated by structural improvements to favour the attack of Cys residue to the carbonyl carbon or the β-carbon. More potent Michael acceptor inhibitors of rhodesain can be based on compounds with more than one reactive position.

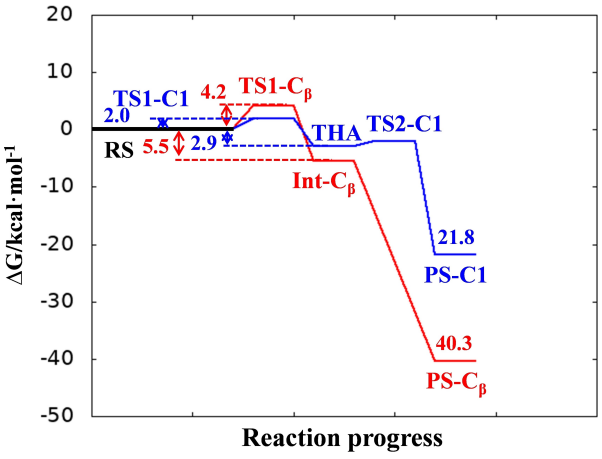

Figure 5. Free-energy profiles corresponding to the inhibition mechanisms of rhodesain cysteine protease by the dipeptidyl enoate Cbz-Phe-Leu-CH=CH–$CO_2C_2H_5$. The red line corresponds to the mechanism I while the blue line corresponds to the mechanism II. The profiles were derived from the FESs computed at the M06-2X/6-31+G(d,p):AM1d/MM level of theory.

With respect to the hydrogen-bonding interactions between the inhibitor and the residues of the active site measured in the structures of the key states generated in the exploration of both inhibition mechanisms, the strong interaction between His159 and Asn175 (see Tables S2 and S3) must be related to their low free-energy barriers, confirming the important role of the active-site Asn175 residue to stabilize the His159 residue.[17,37] An important number of hydrogen-bonding interactions between the inhibitor and the residues of the active site are detected; the strong interaction between the residues Gly66 and Asp158 and the inhibitor during the whole inhibition process (see distances H2-O_{Gly66} and H1-O_{Asp158} in Tables S2 and S3 in the Supporting Information) shows the high affinity of the inhibitor, in total agreement to the results obtained by Schirmeister and co-workers.[31] Hydrogen-bonding interactions between the inhibitor and the residues Gln19, Trp26, Gly66, Asp158, and Trp177 are present during the whole inhibition process.

As commented in the Introduction, the inhibition of rhodesain depends on the peptidic framework of the inhibitor.[5,6,10,28–34] In order to perform a more detailed analysis of this dependency, the QM/MM interaction energies (electrostatic plus Lennard-Jones) between residues of rhodesain and the inhibitor were computed as an average over 10000 structures from the AM1d/MM simulations (see Figures from S4, S5, S7 and S8 in the Supporting Information). The main favourable rhodesain-inhibitor interactions in the RS state of both inhibition mechanisms is shown in Figure 6. In general, the large number of stabilizing interactions with the S2 pocket of the enzyme suggests that P2 is the most important fragment to consider in the design of new efficient inhibitors of rhodesain. Residues of the S2 pocket, such as Trp26, Gly66 and Asp158, interact and stabilize the inhibitor through strong hydrogen bond interactions. Other residues of the S2 pocket of the enzyme, Leu67, Met68 and Leu157, do not form binding interactions but establish stabilizing interaction with the Phe residue of the inhibitor. No major favourable interactions with the S1 pocket of the enzyme were observed.

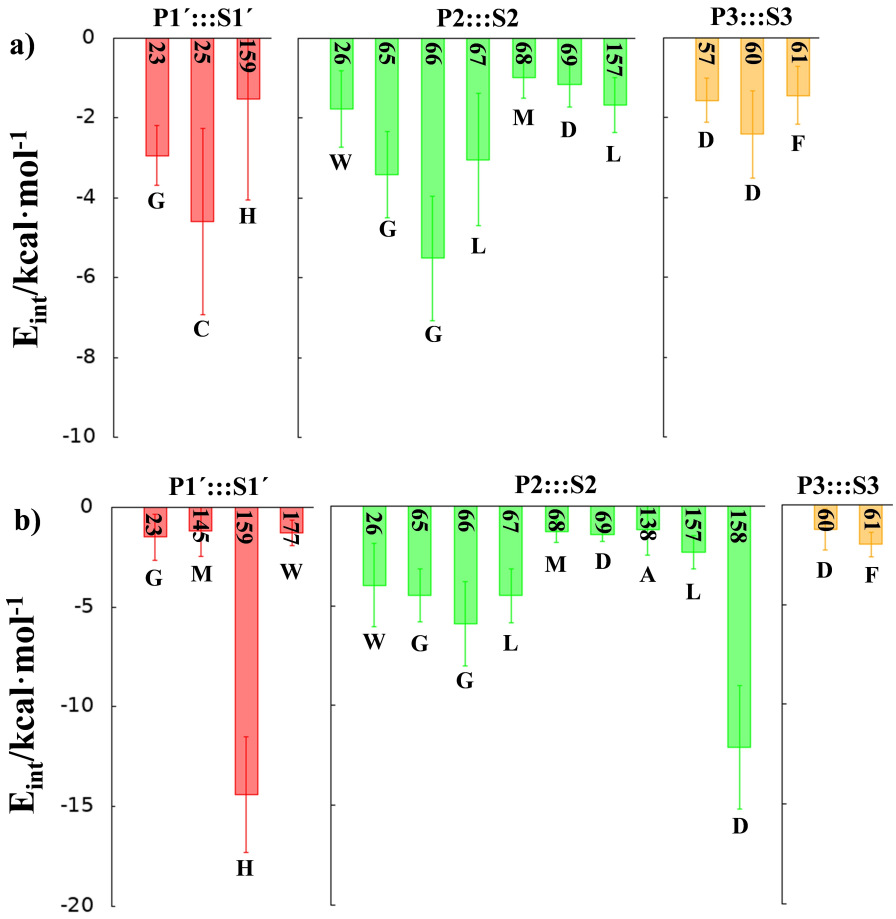

Figure 6. Main favourable average interaction energies (electrostatic plus Lennard-Jones) between residues of rhodesain and each fragment of the inhibitor computed in the RS state of both inhibition mechanism I (a) and mechanism II (b). Results obtained as an average over 10000 structures of the AM1d/MM MD simulations.

Conclusions

A computational study of the two possible inhibition mechanisms of rhodesain cysteine protease by the dipeptidyl enoate Cbz-Phe-Leu-CH=CH–$CO_2C_2H_5$ has been carried out by means of MD simulations with hybrid QM/MM potentials, the nucleophilic attack of Cys25 on the C_β of the inhibitor (Mechanism I) or the carbonyl carbon C1 of the inhibitor (Mechanism II). The first conclusion derived from our study is that the Cys25 residue can attack both C_β and C1 atoms of the inhibitor, confirming a dual mode of action in the inhibition of the rhodesain by the enoates, suggested by one of us.[5] According to our results, both inhibition mechanisms take place in two steps; the first step is related to the formation of the SG–C bond, forming stable intermediates, Int-C_β and THA in mechanism I and II, respectively. From both the kinetic and thermodynamic point of views, the formation of these intermediates is a favourable and reversible process. The low activation free energies obtained in both alkylation process are consistent with the second-order rate constant determined by González and co-workers.[10] The second step of the two inhibition mechanisms consist in the protonation of the intermediates, Int-C_β and THA, by means of a proton transfer from His159 to the C_α atom (Int-C_β) or the O1 atom (THA) of the inhibitor leading to the formation of the PS-C_β and PS–C1 complexes, respectively. According to the energy required for the decomposition of these intermediates into products, this second step is kinetically irrelevant and THA can be considered as a metastable intermediate. Nevertheless, the significant difference in the second step of both inhibition mechanisms is related to its reversibility; while the formation of the PS-C_β complex is an irreversible process, the formation of the PS–C1 complex is a reversible process. In summary, the full inhibition process through the Cys25 attack on the C_β atom of the inhibitor is exergonic and irreversible with a value of the reaction free energy of −40.3 kcal·mol^{-1}; and full inhibition process through the Cys25 attack on the C1 atom of the inhibitor is exergonic and reversible with a value of the reaction free energy of −21.8 kcal·mol^{-1}, confirming a dual mode of action of this family of inhibitors, as previously suggested by González and co-workers.[5]

Concerning the interactions between the residues of the active site and the inhibitor, an important number of hydrogen-bonding interactions are detected. In particular, interactions

between residues Gln19, Trp26, Gly66, Asp158, and Trp177 appear to be important during the whole inhibition process and confirm the great affinity of the inhibitor.[31] In addition, the strong interaction between the His159 and Asn175 observed in both inhibition mechanisms can be related to their low free-energy barriers, confirming the important role of the active-site Asn175 residue to stabilize the His159 residue.[17,37] Analysis of the QM/MM interaction energies between the peptidic framework of the inhibitor and the residues of rhodesain, suggest that P2 is the most important fragment to consider in the design of new efficient inhibitors of rhodesain. The interactions between the inhibitor and rhodesain are clearly dominated by those in the P2:::S2 site. Residues that interact with the inhibitor through strong hydrogen-bonding interactions, as Trp26, Gly66, and Asp158, form stabilizing interactions with the P2 pocket of the inhibitor. Other residues of the S2 pocket of the enzyme, Leu67, Met68 and Leu157, do not form binding interactions but establish stabilizing interaction with the Phe residue of the inhibitor. These results may be useful for the design of new inhibitors of rhodesain with greater selectivity and affinity, by increasing the interaction with the S2 pocket of rhodesain. The confirmation of the dual mode of action of this family of inhibitors is an important issue that can be used to design improved inhibitors whose reversible or irreversible character could be modulated by structural improvements to favour the attack of Cys residue to the carbonyl carbon or the β-carbon. More potent Michael acceptor inhibitors of rhodesain can be based on compounds with more than one reactive position.

These conclusions suggest that dipeptidyl enoates derivatives can be also used to inhibit other cysteine proteases related with human diseases.

Computational Methods

The starting structure for the construction of the rhodesain-inhibitor model was the X-ray crystal structure of rhodesain from *Trypanosoma brucei rhodesiense* with PDB code 2P7 U.[38] The bound inhibitor K777 was replaced with the enoate inhibitor Cbz-Phe-Leu-CH=CH–$CO_2C_2H_5$. This particular X-ray structures was already used in our laboratory to carry out computational studies on the inhibition of rhodesain cysteine proteases by dipeptidyl nitroalkenes.[17]

In the molecular model, the missing hydrogen atoms of the X-ray structure were added at pH 7 using the tLEAP module[39] of Amber Tools program within the pK_a values of the titratable residues calculated within the empirical PROPKA 3.1 program.[40] Missing force field parameters for the inhibitor were computed using Antechamber software.[41] Neutralization of the system was achieved by adding 16 Na^+ counterions in the electrostatically most favourable positions. Finally, the system was solvated in an orthorhombic box of TIP3P[42] water molecules with the following size: 75.5×79.4×77.1 Å^3. 10 ns of classical MD simulations were required to equilibrate the system using the AMBER force field[43] implemented in NAMD software.[44] The MD simulations were carried out at 300 K using the NVT ensemble with a time step of 1 fs. The temperature during the MD simulation was controlled using the Langevin thermostat.[45] Analysis of the time evolution of the root-mean-square deviation of the backbone atoms of the protein models confirms that the system was equilibrated (see Figure S1 in the Supporting Information). Analysis was done using cpptraj software.[46]

Once the molecular model was set up and equilibrated, potential energy surfaces (PESs) corresponding to every possible chemical step of the inhibition mechanisms were explored. The reactants, products, intermediates and transition state structures were optimized by means of a micro-macro iterations scheme.[47] Frequency calculations were carried out in all located structures to characterize them as minima or saddle points of order one. The fDYNAMO library[48] was used for the QM/MM calculations. The QM region was initially described with the AM1d semiempirical Hamiltonian,[49] and contains the full inhibitor, the residue Cys25, the imidazole ring of His159 (see Figure 7a). This is the Hamiltonian already employed in different computational studies related to the cysteine proteases carried out in our laboratory.[17,23–25,50,51] The rest of the system, protein and water molecules, were described by the OPLS-AA[52] and TIP3P[42] force fields, respectively. Hydrogen link atoms were used to saturate the valence of the QM-MM frontier bonds (see Figure 7a).[53] All residues further than 25 Å from the C_β atom of the inhibitor were kept frozen during the simulations. A force switching function with a cut-off distance in the range of 14.5 to 16 Å and periodic boundary conditions were employed to treat the non-bonding interactions.

Once the PESs were obtained (see Figures S2 and S6a in the Supporting Information), FESs were generated in terms of the PMF using umbrella sampling and the weighted histogram analysis

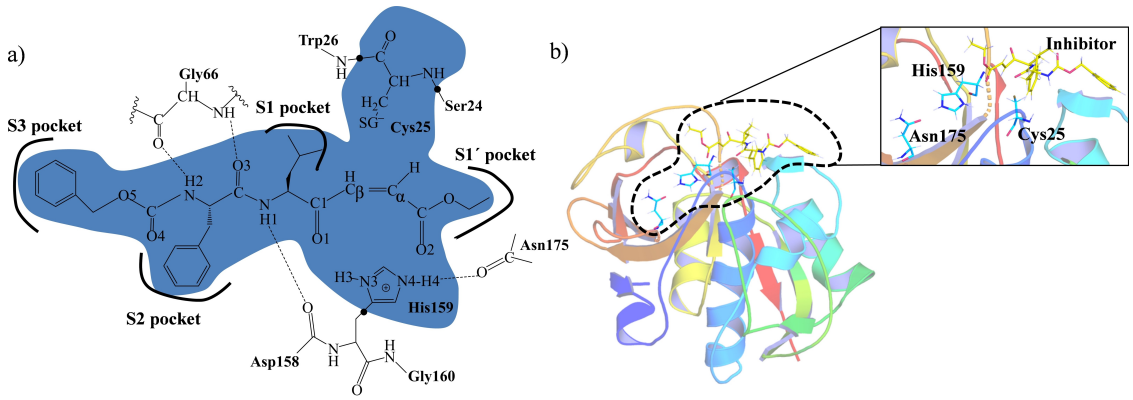

Figure 7. a) Details of the atoms of the active site treated quantum mechanically (blue region). The link atoms between the QM and MM regions are indicated as black dots. b) Representative rhodesain-inhibitor model.

method to recover the probabilities.[54,55] The error associated to this method, when properly carried out, is usually accepted to be around 1 kcal·mol^{-1}.[56] The harmonic umbrella sampling force constants was 2500 kJ·mol^{-1}·Å^{-2}. 20 ps of equilibration and 40 ps of production, with a time step of 1 fs, were used in every window of the PMFs.

For the study of the mechanism I, a monodimensional PMF (1D-PMF) was generated using the bond-forming distance, d(SG-C$_\beta$), as the reaction coordinate, ζ, to monitor the attack of the sulfur atom of Cys25 on the C$_\beta$ of the inhibitor (see Figure S3a). This required series of 68 simulation windows. This step leads to an intermediate called Int-C$_\beta$. For the protonation of the Int-C$_\beta$ intermediate, a 1D-PMF (see Figure S3b) was generated using as ζ the antisymmetric combination of two distances defining the hydrogen transfer from the His159 to the C$_\alpha$ of the inhibitor, d(N3-H3)-d(C$_\alpha$-H3). This step required series of 63 simulation windows. And finally, for the study of the mechanism II, a 2D-PMF was generated with the bond-forming distance between Cys25 and C1 carbonyl carbon atom of the inhibitor, d(SG–C1) as ζ_1, and the antisymmetric combination of the two distances defining the hydrogen transfer from the His159 to the O1 of the inhibitor, d(N3-H3)-d(O1-H3), as ζ_2 (see Figure S6b). This required series of 2211 simulation windows centred on the values of the previously generated PES. The QM sub-set of atoms in the QM/MM FESs were restricted to a low-level Hamiltonian, AM1d, because of computer limitations. In order to improve the level of theory, an interpolated correction scheme with a higher level Hamiltonian, developed in our laboratory,[57] was applied as explained in detail in our previous papers.[17,23–25,50,51] The M06-2X functional[58] with the standard 6–31+G(d,p) basis set,[59] following Truhlar and co-workers suggestions,[58,60] was used employing the *Gaussian09* program,[61] combined with the fDYNAMO library.[48]

Finally, in order to obtain averaged interaction energies between the enzymatic environment and the inhibitor, 1 ns of AM1d/MM MD simulations of the windows corresponding to the different states were performed.

Contribution of each residue of the protein to the interaction energy with defined part of inhibitor was computer using the following expression:

$$E^{Int}_{QM/MM} = \sum \langle \Psi | \frac{q_{MM}}{r_{e,MM}} | \Psi \rangle + \sum \sum \frac{Z_{QM} q_{MM}}{r_{QM,MM}} + E^{vdW}_{QM/MM} \quad (1)$$

This interaction energy can be exactly decomposed in a sum over residues provided that the polarized wave function (Ψ) is employed to evaluate this energy contribution. The global polarization effect can be obtained from the gas phase energy difference between the polarized, Ψ, and non-polarized, Ψ_0, wave functions.

Supporting Information

RMSD computed along the classical MD simulation for the backbone atoms of the protein; PESs and FESs computed at AM1d/MM level corresponding to every single step of the different inhibition mechanisms; key average inter-atomic distances for the key states located along the different inhibition mechanisms, average interaction energies by residues for some key states for the reaction mechanisms, and Cartesian coordinates of the QM subset of atoms of the TSs, RSs, Int-C$_\beta$, THA and PS–C1 optimized at M06-2X/6-31+G(d,p)/MM level.

Acknowledgements

This work was supported by the Spanish Ministerio de Ciencia, Innovación y Universidades (PGC2018-094852-B-C21), Generalitat Valenciana (AICO/2019/195) Universitat Jaume I (UJI-B2020-03). K.A. thanks Generalitat Valenciana (APOSTD/2020/015) for post-doctoral contract. The authors thankfully acknowledge the local computational resources of the Servei d'Informàtica of Universitat Jaume I.

Conflict of Interest

The authors declare no conflict of interest.

Keywords: free energy surfaces · dipeptidyl enoates · inhibition mechanism · molecular dynamics · rhodesain · QM/MM

[1] H. A. Chapman, R. J. Riese, G.-P. Shi, *Annu. Rev. Physiol.* **1997**, *59*, 63–88.
[2] J. H. McKerrow, J. C. Engel, C. R. Caffrey, *Bioorg. Med. Chem.* **1999**, *7*, 639–644.
[3] V. Olga, R. Thomas, P. Christoph, T. Dusan, T. Vito, T. Boris, *Curr. Pharm. Des.* **2007**, *13*, 387–403.
[4] https://www.who.int/news-room/fact-sheets/detail/trypanosomiasis-human-african-(sleeping-sickness)/ (accessed March 2021).
[5] S. Royo, S. Rodriguez, T. Schirmeister, J. Kesselring, M. Kaiser, F. V. Gonzalez, *ChemMedChem* **2015**, *10*, 1484–1487.
[6] A. Latorre, T. Schirmeister, J. Kesselring, S. Jung, P. Johe, U. A. Hellmich, A. Heilos, B. Engels, R. L. Krauth-Siegel, N. Dirdjaja, L. Bou-Iserte, S. Rodriguez, F. V. Gonzalez, *ACS Med. Chem. Lett.* **2016**, *7*, 1073–1076.
[7] S. F. P. Braga, L. C. Martins, E. B. da Silva, P. A. Sales, S. M. F. Murta, A. J. Romanha, W. T. Soh, H. Brandstetter, R. S. Ferreira, R. B. de Oliveira, *Bioorg. Med. Chem.* **2017**, *25*, 1889–1900.
[8] M. Giroud, B. Kuhn, S. Saint-Auret, C. Kuratli, R. E. Martin, F. Schuler, F. Diederich, M. Kaiser, R. Brun, T. Schirmeister, W. Haap, *J. Med. Chem.* **2018**, *61*, 3370–3388.
[9] D. A. Rocha, E. B. Silva, I. S. Fortes, M. S. Lopes, R. S. Ferreira, S. F. Andrade, *Eur. J. Med. Chem.* **2018**, *157*, 1426–1459.
[10] S. Royo, T. Schirmeister, M. Kaiser, S. Jung, S. Rodriguez, J. Manuel Bautista, F. V. Gonzalez, *Bioorg. Med. Chem.* **2018**, *26*, 4624–4634.
[11] P. Klein, P. Johe, A. Wagner, S. Jung, J. Kuhlborn, F. Barthels, S. Tenzer, U. Distler, W. Waigel, B. Engels, U. A. Hellmich, T. Opatz, T. Schirmeister, *Molecules* **2020**, *25*.
[12] D. Steverding, *Molecules* **2020**, *25*, 143.
[13] P. S. Doyle, Y. M. Zhou, J. C. Engel, J. H. McKerrow, *Antimicrob. Agents Chemother.* **2007**, *51*, 3932–3939.
[14] J. T. Palmer, D. Rasnick, J. L. Klaus, D. Bromme, *J. Med. Chem.* **1995**, *38*, 3193–3196.
[15] R. P. Hanzlik, S. A. Thompson, *J. Med. Chem.* **1984**, *27*, 711–712.
[16] J. C. Powers, J. L. Asgian, O. D. Ekici, K. E. James, *Chem. Rev.* **2002**, *102*, 4639–4750.
[17] K. Arafet, F. V. González, V. Moliner, *Chem. Eur. J.* **2020**, *26*, 2002–2012.
[18] K. Arafet, N. Serrano-Aparicio, A. Lodola, A. J. Mulholland, F. V. González, K. Świderek, V. Moliner, *Chem. Sci.* **2021**, *12*, 1433–1444.
[19] A. E. Howard, P. A. Kollman, *J. Am. Chem. Soc.* **1988**, *110*, 7195–7200.
[20] D. Arad, R. Langridge, P. A. Kollman, *J. Am. Chem. Soc.* **1990**, *112*, 491–502.
[21] K. Byun, J. L. Gao, *J. Mol. Graphics Modell.* **2000**, *18*, 50–55.
[22] D. H. Wei, X. Q. Huang, J. J. Liu, M. S. Tang, C. G. Zhan, *Biochemistry* **2013**, *52*, 5145–5154.
[23] K. Arafet, S. Ferrer, V. Moliner, *Biochemistry* **2015**, *54*, 3381–3391.
[24] K. Arafet, S. Ferrer, V. Moliner, *ACS Catal.* **2017**, *7*, 1207–1215.
[25] K. Arafet, K. Świderek, V. Moliner, *ACS Omega* **2018**, *3*, 18613–18622.
[26] L. Zhang, D. Lin, X. Sun, U. Curth, C. Drosten, L. Sauerhering, S. Becker, K. Rox, R. Hilgenfeld, *Science* **2020**, *368*, 409–412.
[27] K. Świderek, V. Moliner, *Chem. Sci.* **2020**, *11*, 10626–10630.

[28] V. Ehmke, E. Winkler, D. W. Banner, W. Haap, W. B. Schweizer, M. Rottmann, M. Kaiser, C. Freymond, T. Schirmeister, F. Diederich, *ChemMedChem* **2013**, *8*, 967–975.
[29] R. Ettari, S. Previti, S. Cosconati, J. Kesselring, T. Schirmeister, S. Grasso, M. Zappala, *J. Enzyme Inhib. Med. Chem.* **2016**, *31*, 1184–1191.
[30] S. Previti, R. Ettari, S. Cosconati, G. Arnendola, K. Chouchene, A. Wagner, U. A. Hellmich, K. Ulrich, R. L. Krauth-Siegel, P. R. Wich, I. Schmid, T. Schirmeister, J. Gut, P. J. Rosenthal, S. Grasso, M. Zappala, *J. Med. Chem.* **2017**, *60*, 6911–6923.
[31] T. Schirmeister, J. Schmitz, S. Jung, T. Schmenger, R. L. Krauth-Siegel, M. Guetschow, *Bioorg. Med. Chem. Lett.* **2017**, *27*, 45–50.
[32] L. H. Santos, B. J. Waldner, J. E. Fuchs, G. A. N. Pereira, K. R. Liedl, E. R. Caffarena, R. S. Ferreira, *J. Chem. Inf. Model.* **2019**, *59*, 137–148.
[33] R. Ettari, S. Previti, S. Maiorana, G. Amendola, A. Wagner, S. Cosconati, T. Schirmeister, U. A. Hellmich, M. Zappalà, *J. Med. Chem.* **2019**, *62*, 10617–10629.
[34] S. Maiorana, R. Ettari, S. Previti, G. Amendola, A. Wagner, S. Cosconati, U. A. Hellmich, T. Schirmeister, M. Zappalà, *ChemMedChem* **2020**, *15*, 1552–1561.
[35] H. Zhang, J. Collins, R. Nyamwihura, O. Crown, O. Ajayi, I. V. Ogungbe, *Bioorg. Med. Chem. Lett.* **2020**, *30*.
[36] P. Johe, S. Jung, E. Endres, C. Kersten, C. Zimmer, W. Ye, C. Sönnichsen, U. A. Hellmich, C. Sotriffer, T. Schirmeister, H. Neuweiler, *ACS Chem. Biol.* **2021**.
[37] T. Vernet, D. C. Tessier, J. Chatellier, C. Plouffe, T. S. Lee, D. Y. Thomas, A. C. Storer, R. Ménard, *J. Biol. Chem.* **1995**, *270*, 16645–16652.
[38] I. D. Kerr, J. H. Lee, C. J. Farady, R. Marion, M. Rickert, M. Sajid, K. C. Pandey, C. R. Caffrey, J. Legac, E. Hansell, J. H. McKerrow, C. S. Craik, P. J. Rosenthal, L. S. Brinen, *J. Biol. Chem.* **2009**, *284*, 25697–25703.
[39] C. E. A. F. Schafmeister, W. S. Ross, V. Romanovski, *University of California, San Francisco* **1995**.
[40] M. H. M. Olsson, C. R. Sondergaard, M. Rostkowski, J. H. Jensen, *J. Chem. Theory Comput.* **2011**, *7*, 525–537.
[41] J. Wang, W. Wang, P. A. Kollman, D. A. Case, *J. Mol. Graphics Modell.* **2006**, *25*, 247–260.
[42] W. L. Jorgensen, J. Chandrasekhar, J. D. Madura, R. W. Impey, M. L. Klein, *J. Chem. Phys.* **1983**, *79*, 926–935.
[43] Y. Duan, C. Wu, S. Chowdhury, M. C. Lee, G. M. Xiong, W. Zhang, R. Yang, P. Cieplak, R. Luo, T. Lee, J. Caldwell, J. M. Wang, P. Kollman, *J. Comput. Chem.* **2003**, *24*, 1999–2012.
[44] J. C. Phillips, R. Braun, W. Wang, J. Gumbart, E. Tajkhorshid, E. Villa, C. Chipot, R. D. Skeel, L. Kalé, K. Schulten, *J. Comput. Chem.* **2005**, *26*, 1781–1802.
[45] G. S. Grest, K. Kremer, *Phys. Rev. A* **1986**, *33*, 3628–3631.
[46] D. R. Roe, T. E. Cheatham, *J. Chem. Theory Comput.* **2013**, *9*, 3084–3095.
[47] S. Martí, V. Moliner, I. Tuñón, *J. Chem. Theory Comput.* **2005**, *1*, 1008–1016.
[48] M. J. Field, M. Albe, C. Bret, F. Proust-De Martin, A. Thomas, *J. Comput. Chem.* **2000**, *21*, 1088–1100.
[49] K. Nam, Q. Cui, J. Gao, D. M. York, *J. Chem. Theory Comput.* **2007**, *3*, 486–504.
[50] K. Arafet, S. Ferrer, S. Martí, V. Moliner, *Biochemistry* **2014**, *53*, 3336–3346.
[51] K. Arafet, S. Ferrer, F. V. Gonzalez, V. Moliner, *Phys. Chem. Chem. Phys.* **2017**, *19*, 12740–12748.
[52] W. L. Jorgensen, D. S. Maxwell, J. TiradoRives, *J. Am. Chem. Soc.* **1996**, *118*, 11225–11236.
[53] M. J. Field, P. A. Bash, M. Karplus, *J. Comput. Chem.* **1990**, *11*, 700–733.
[54] S. Kumar, D. Bouzida, R. H. Swendsen, P. A. Kollman, J. M. Rosenberg, *J. Comb. Chem.* **1992**, *13*, 1011–1021.
[55] G. M. Torrie, J. P. Valleau, *J. Comput. Phys.* **1977**, *23*, 187–199.
[56] J. Kästner, W. Thiel, *J. Chem. Phys.* **2006**, *124*, 234106.
[57] J. J. Ruiz-Pernia, E. Silla, I. Tuñón, S. Martí, V. Moliner, *J. Phys. Chem. B* **2004**, *108*, 8427–8433.
[58] Y. Zhao, D. G. Truhlar, *Theor. Chem. Acc.* **2008**, *120*, 215–241.
[59] W. J. Hehre, L. Radom, P. V. R. Schleyer, J. A. Pople, *Ab Initio Molecular Orbital Theory*, Wiley, New York, **1986**.
[60] B. J. Lynch, X. Zhao, D. G. Truhlar, *J. Phys. Chem. A* **2003**, *107*, 1384–1388.
[61] Gaussian 09 (Revision A.1), M. J. Frisch, G. W. Trucks, H. B. Schlegel, G. E. Scuseria, M. A. Robb, J. R. Cheeseman, G. Scalmani, V. Barone, B. Mennucci, G. A. Petersson, H. Nakatsuji, X. L. M. Caricato, H. P. Hratchian, A. F. Izmaylov, J. Bloino, G. Zheng, J. L. Sonnenberg, M. Hada, M. Ehara, K. Toyota, R. Fukuda, J. Hasegawa, M. Ishida, T. Nakajima, Y. Honda, O. Kitao, H. Nakai, T. Vreven, J. A. Montgomery Jr., J. E. Peralta, F. Ogliaro, M. Bearpark, J. J. Heyd, E. Brothers, K. N. Kudin, V. N. Staroverov, R. Kobayashi, J. Normand, K. Raghavachari, A. Rendell, J. C. Burant, S. S. Iyengar, J. Tomasi, M. Cossi, N. Rega, J. M. Millam, M. Klene, J. E. Knox, J. B. Cross, V. Bakken, C. Adamo, J. Jaramillo, R. Gomperts, R. E. Stratmann, O. Yazyev, A. J. Austin, R. Cammi, C. Pomelli, J. W. Ochterski, R. L. Martin, K. Morokuma, V. G. Zakrzewski, G. A. Voth, P. Salvador, J. J. Dannenberg, S. Dapprich, A. D. Daniels, Ö. Farkas, J. B. Foresman, J. V. Ortiz, J. Cioslowski, D. J. Fox, **2009**.

Manuscript received: March 10, 2021
Accepted manuscript online: April 14, 2021
Version of record online: May 27, 2021

